A Facile Synthesis–Fabrication Strategy for Integration of Catalytically Active Viral-Palladium Nanostructures into Polymeric Hydrogel Microparticles *via* Replica Molding

Cuixian Yang,[†] Chang-Hyung Choi,[‡] Chang-Soo Lee,[‡] and Hyunmin Yi[†,*]

[†]Department of Chemical and Biological Engineering, Tufts University, Medford, Massachusetts 02155, United States and [‡]Department of Chemical Engineering, Chungnam National University, Daejeon 305-764, Republic of Korea

ABSTRACT The synthesis of small, uniform, well-dispersed and active Pd nanocatalysts under mild conditions in a predictable and controlled manner is an unmet challenge. Viral nanomaterials are attractive biotemplates for the controlled synthesis of nanoparticles due to their well-defined and monodisperse structure along with abundant surface functionalities. Here, we demonstrate spontaneous formation of small (1–2 nm), uniform and highly crystalline palladium (Pd) nanoparticles along genetically modified tobacco mosaic virus (TMV1cys) biotemplates without external reducing agents. The ratio between TMV and Pd precursor plays an important role in the exclusive formation of well-dispersed Pd nanoparticles along TMV biotemplates. The as-prepared Pd–TMV complexes are then integrated into the poly(ethylene glycol) (PEG)-based microparticles *via* replica molding (RM) technique in a simple, robust and highly reproducible manner. High catalytic activity, recyclability and stability of the hybrid Pd–TMV–PEG microparticles are further demonstrated through dichromate reduction as a model reaction. Taken together, these findings demonstrate a significant step toward simple, robust, and scalable synthesis and fabrication of efficient biotemplate-supported Pd nanocatalysts in readily deployable polymeric scaffolds with high capacity in a controlled manner.

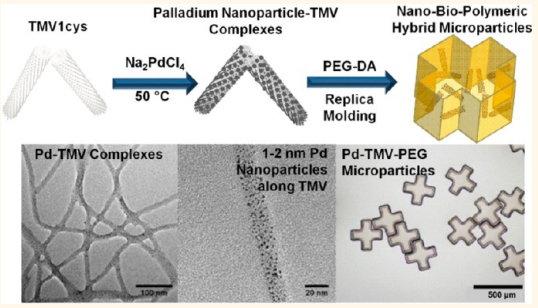

KEYWORDS: tobacco mosaic virus · palladium nanocatalysts · nano-bio-polymeric hybrid · PEG microparticles · dichromate reduction

Metal nanoparticles play an important role in catalysis due to their irregular surfaces, high surface-to-volume ratio and size-dependent properties, which can be tuned to optimize catalytic activity and selectivity. Palladium (Pd) is an important precious metal catalyst useful for a wide range of chemical reactions.[1–3] The synthesis of small, uniform, well-dispersed and catalytically active Pd nanoparticles under mild conditions in a predictable and controlled manner is an unmet challenge, despite recent developments in the dispersion and stabilization of Pd nanoparticles.[4–9] Meanwhile, biological supramolecules such as viruses[10–15] and protein cages[16–18] have gained substantial attention as alternative template materials for the controlled synthesis of metal and metal oxide nanoparticles due to their well-defined structure, monodispersed dimensions, and abundant surface functionalities that can be further modified *via* chemical and/or genetic modifications. Particularly, Tobacco Mosaic Virus (TMV) has been extensively utilized due to their robust tubular structure and stability in a wide range of conditions (*e.g.*, pH between 2 and 10, temperature up to 90°C and organic solvents such as 80% ethanol) as well as safety and simple mass production.[19–23] Also, genetically displayed cysteines on TMV coat proteins (such as TMV1cys or TMV2cys) have been shown to improve Pd nanoparticle formation rising from the enhanced biosorption of the precursors.[24–26] However, the use of reducing agents (*e.g.*, dimethylamine borane (DMAB), sodium borohydride ($NaBH_4$))

* Address correspondence to hyunmin.yi@tufts.edu.

Received for review February 1, 2013 and accepted May 21, 2013.

Published online May 23, 2013
10.1021/nn4005582

leads to large and often uncontrollable Pd nanoparticle formation, with a few exceptions such as on surface-assembled formats,[27−30] resulting in inefficient use of the expensive metal precursors for potential applications such as catalysis. Recently, Lim *et al.*[31,32] reported the controlled synthesis of Pd coatings with thickness of 25−35 nm on TMV biotemplates in the absence of reducing agents. While these studies present potential for the controlled synthesis of functional nanomaterials, substantially smaller and well-dispersed nanoparticles are required for catalytic applications. For example, compared with larger nanoparticles, 1−2 nm Pd nanoparticles supported in large pores of mesocellular foam with lower metal loading showed higher selectivity and reactivity for amine racemization.[33]

In the meantime, seamless integration of novel nanocatalysts with robust platforms that confer stability, scalable production, and ease of separation and recovery while allowing for ready access of the reactants remains a formidable challenge. Polymeric supports, especially in the form of porous 3D microparticle formats, should provide improved molecular interactions and offer a hydrophilic environment with more favorable solution kinetics.[34] The ability to customize specific microparticle features, such as controlled dimensions, anisotropic shapes and added functionalities (*e.g.*, magnetic properties),[35,36] would further enhance the utility of the catalysts integrated in such hybrid materials as alternative means for separation from bulk solution, patterning, or self-assembly. Recently, polymeric hydrogels have been used as stabilizing platforms for viral or metal nanoparticles, and even served as effective templates for the *in situ* synthesis of metal nanocatalysts[37−40] (*e.g.*, Co, Ni, Cu, Ag) for chemical reactions. Particularly, poly(ethylene glycol) (PEG) with long chain length has been emerging as both reducer and stabilizer for the synthesis of Pd nanoparticles in the studies of aerobic alcohol oxidation,[41,42] selective hydrogenation reaction[43,44] and Heck reaction.[45] PEG is relatively inexpensive, non-volatile, nontoxic and environmentally benign. In addition, the physical properties (*e.g.*, mesh size) of PEG-based hydrogels can be readily controlled simply by varying the molecular weight and structure (linear *vs* branched) of the PEG used.[46] Thus, PEG-based hydrogels present significant potential as stabilizers or matrixes for the fabrication of functional materials with catalytic activities.

In this study, we demonstrate a simple approach for the synthesis of small, uniform and highly active Pd nanocatalysts on TMV1cys biotemplates (Pd−TMV) in the absence of reducing agents. We also demonstrate that these novel nano-bio materials can be readily integrated into PEG hydrogel microparticle platforms *via* a simple and robust replica molding (RM)-based fabrication technique. As shown in the schematic diagram of Figure 1, our synthesis-fabrication

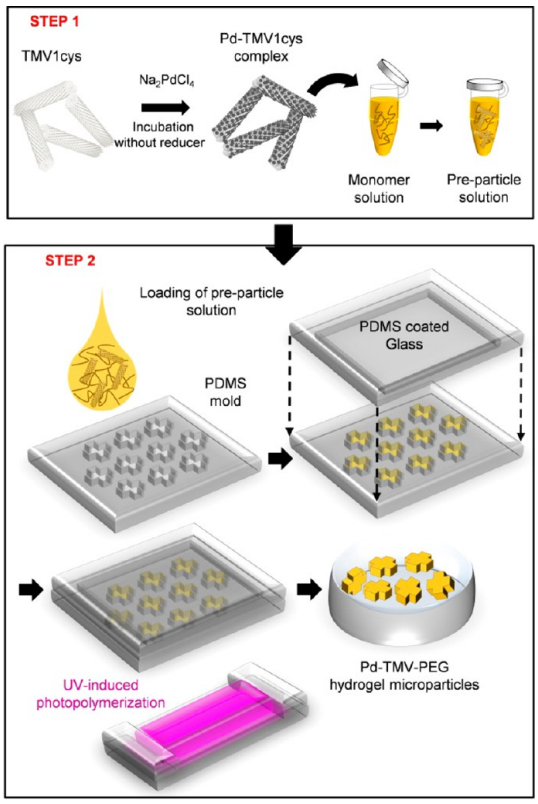

Figure 1. Synthesis of Pd−TMV Encapsulated PEG-based microparticles by Replica Molding (RM) (Step 1: spontaneous formation of Pd nanoparticle without reducing agent. Step 2: fabrication of PEG-based microparticle *via* replica molding technique.).

procedure consists of two steps. First, simple mixing of TMV with the Pd precursor (Na_2PdCl_4) solution at 50 °C leads to rapid and spontaneous formation of small (1−2 nm), uniform, well-dispersed and highly crystalline Pd nanoparticles along TMV biotemplates without reducer in aqueous solution (Step 1). In-depth analysis *via* Transmission Electron Microscopy (TEM) shows that the concentrations of Pd precursor and TMV as well as the ratio between these two are important factors for the uniform and exclusive formation of Pd nanoparticles along TMV biotemplates. Second, the as-prepared Pd−TMV complexes are readily integrated into PEG polymeric hydrogel microparticles *via* a simple and robust replica molding (RM) technique (Step 2). Specifically, the Pd−TMV complexes are mixed with PEG diacrylate (PEGDA) and photoinitiator to yield the preparticle solution, then placed on PDMS micromolds. Brief irradiation of UV light induces radical chain polymerization[47] to form cross-linked PEG-based hydrogel microparticles containing the Pd−TMV complexes integrated into the polymeric networks in a stable manner (Step 2).

These hybrid microparticles, named Pd−TMV−PEG microparticles, are then utilized for the catalytic reduction of hexavalent chromate ion, a prevalent industrial pollutant in the industrial waste and drinking water

sources.[48] The catalytic reaction study of Pd–TMV–PEG microparticles shows 6-fold higher activity than commercial Pd/C catalysts per Pd mass. Furthermore, results show that the reaction rate is linearly proportional to the Pd loading density inside the Pd–TMV–PEG hydrogel microparticles within the diffusion limitation-free regime. Compared to microfluidic particle fabrication techniques,[49–51] RM allows for simple, robust, scalable and inexpensive integration and manufacturing. In addition, RM technique enables the encapsulation of Pd–TMV complexes in PEG hydrogel microparticles with high Pd loading capacity without clogging or precipitation,[52] commonly found in the microfluidic procedures. Taken together, these results illustrate a facile synthesis-fabrication strategy for robust, highly uniform and catalytically active nanobiopolymeric hybrid materials in a controlled manner. We envision that the results and methods presented in this study can be readily expanded to a variety of other systems for facile fabrication of multifunctional materials with novel nanobio components seamlessly integrated to maximize their functionality and/or stability under relevant working conditions.

RESULTS AND DISCUSSION

Spontaneous Formation of Palladium Nanoparticles along TMV Biotemplates. We first show that small, well-dispersed and highly crystalline palladium (Pd) nanoparticles form on tobacco mosaic virus (TMV) biotemplates in the absence of reducing agent in Figures 2 and 3. First, macroscopic and UV–vis absorbance observations over 30 min incubation period in Figure 2 clearly indicate the conversion of Pd precursors into Pd–TMV complexes that can be readily separated *via* low-speed centrifugation. For this, 10 mM Na_2PdCl_4 (Pd precursor) was mixed with 0.6 mg/mL TMV1cys in deionized (DI) water and incubated at 50 °C for 30 min.

As shown in the photographs of Figure 2a, the color of the solution quickly turned from light yellow to golden yellow within 10 s, then to darker brown yellow slowly over time during the incubation. Next, the UV–vis absorbance spectra in Figure 2b suggest the formation of Pd–TMV complexes. At time zero (solid black line), the UV spectrum of Pd precursor solution shows characteristic absorbance peaks at 320 and 430 nm (marked with solid triangles), which are due to the charge-transfer and d–d transition of $PdCl_3(H_2O)$.[53] Meanwhile, the spectrum also shows very strong absorbance below 300 nm and a small shoulder peak at around 475 nm (marked with solid star), which are due to the presence of $PdCl_4^{2-}$ ions.[53,54] The spectrum of TMV solution (red solid curve) shows TMV's typical absorbance at 260–280 nm (aromatic protein side chains and RNA). After Pd precursor solution was mixed with TMV, those characteristic absorbance peaks of $PdCl_4^{2-}$ and $PdCl_3(H_2O)^-$ become indistinguishable as the incubation proceeds, and are

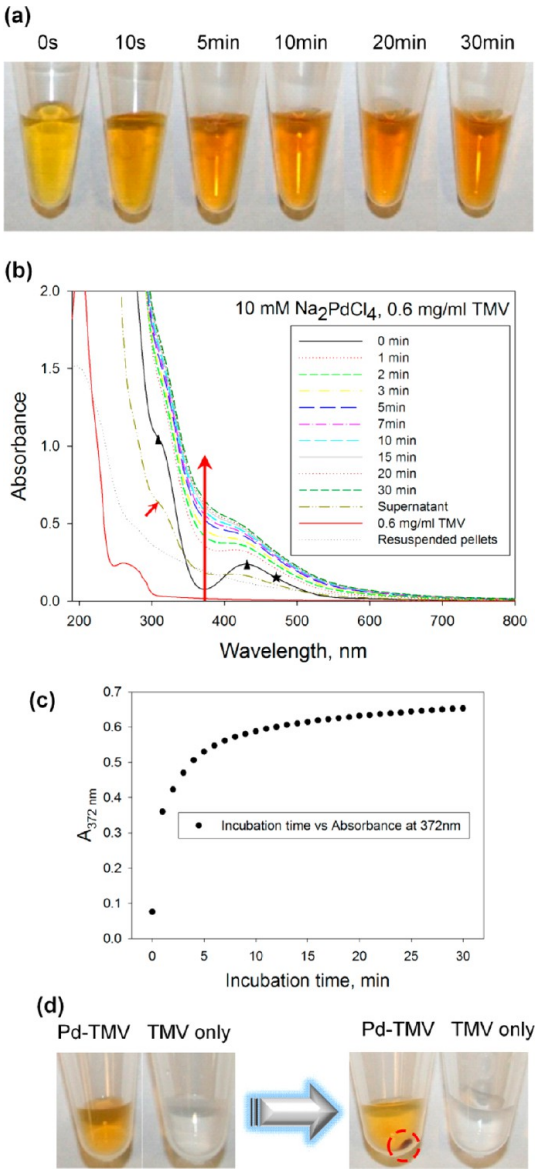

Figure 2. Observation of the formation of Pd–TMV complex with UV–vis spectroscopy. (a) Photographs of Pd–TMV solution over incubation time at 50 °C; (b) UV–vis absorbance of Na_2PdCl_4 solution after mixing with TMV at 50 °C over time (0.1 cm path depth cuvette); (c) A_{372nm} *versus* incubation time; (d) collected Pd–TMV complex pellets by centrifugation. Red dash circle highlights the collected Pd–TMV pellets.

replaced by an increased absorbance over a broad wavelength range. We tracked this change in the spectra by taking the absorbance values at the initial minimum at 372 nm over time, as shown in Figure 2c. This plot suggests that the conversion of the precursor proceeds rapidly within the first five minutes then gradually reaches a plateau under the condition employed in this study. Potential causes of this behavior could be the changes in pH of the solution[31] or the thermodynamic equilibrium in which TMV biotemplates may have reached maximum capacity for the spontaneous formation of Pd nanoparticles, while the exhaustion of the Pd precursor is unlikely as indicated

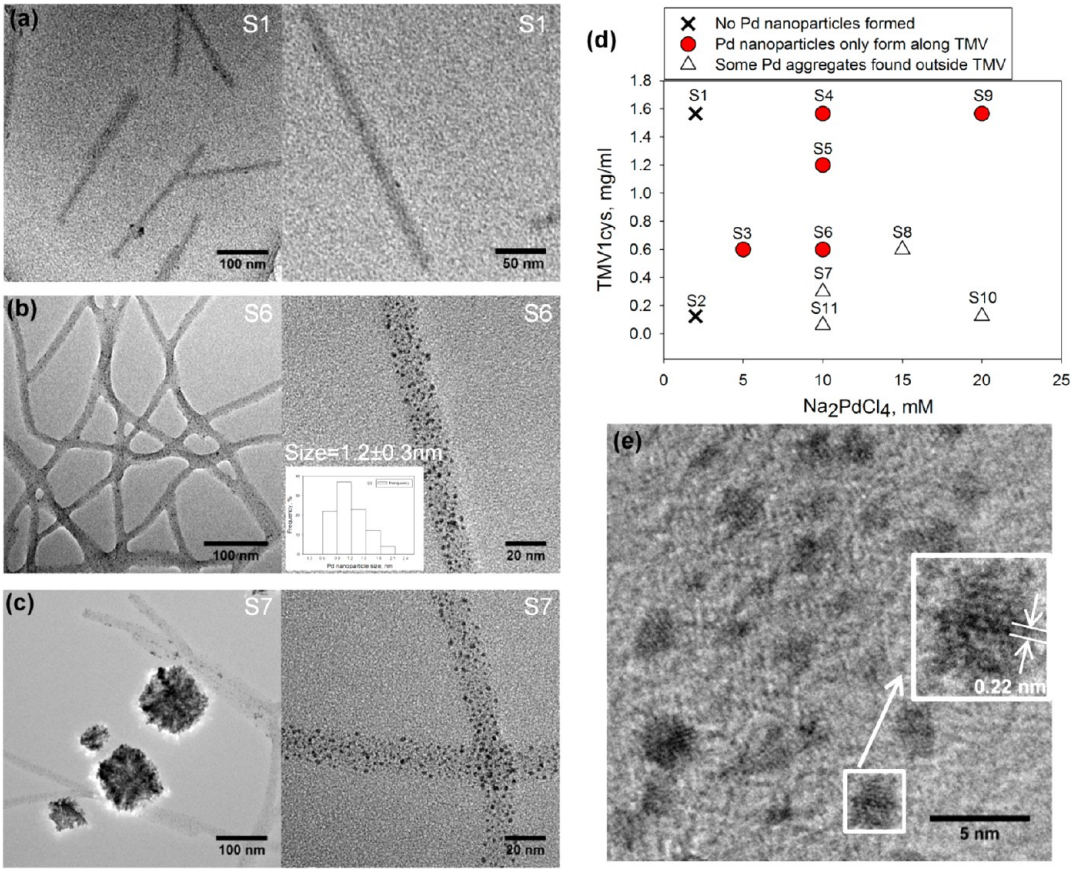

Figure 3. TEM images of spontaneously formed Pd nanoparticles along TMV biotemplates. (a) Sample S1 (2 mM Na_2PdCl_4 and 1.6 mg/mL TMV); (b) sample S6 (10 mM Na_2PdCl_4 and 0.6 mg/mL TMV); (c) sample S7 (10 mM Na_2PdCl_4 and 0.3 mg/mL TMV); (d) the effect of TMV and Na_2PdCl_4 concentrations on the Pd nanoparticle formation along TMV biotemplates; (e) high-resolution TEM image of the crystal structure of Pd nanoparticles (prepared with S6 condition).

by the remaining Pd precursor in the supernatant (double-dotted line with a short arrow in Figure 2b).

Finally, the photographs of Figure 2d show that the Pd–TMV complexes are readily centrifuged at low speed (9000*g*) to yield brown pellets (highlighted with red dash circle) in contrast to TMV solutions that show no pelleting. The UV–vis spectrum of the collected supernatant (double-dotted line with a short arrow) upon 30 min incubation shows similar yet lower absorbance compared to the initial Pd precursor solution, while the resuspended pellets (black dotted line) show apparent shift of absorbance peak into lower wavelength range along with the absence of the 430 nm $PdCl_3(H_2O)^-$ peak, indicating the formation of Pd–TMV complexes.[55] Combined these results in Figure 2 indicate that the Pd–TMV complexes form mostly within the first 5 min.

TEM Characterization. Next, we thoroughly examined the synthesis conditions and the structures of palladium nanoparticles on TMV biotemplates *via* TEM as shown in Figure 3. For this, TMV was exposed to the Pd precursor (Na_2PdCl_4) solution and incubated at 50 °C for 30 min. Upon centrifugation at 9000*g*, the collected pellets were suspended in DI water then placed on the TEM grids.

First, the TEM images of Figure 3a show minimal number of Pd particles for samples prepared with low Pd precursor concentrations (S1: 2 mM Na_2PdCl_4, 1.6 mg/mL TMV). Next, Figure 3b shows that the sample with higher Pd precursor concentrations (S6: 10 mM Na_2PdCl_4, 0.6 mg/mL TMV) exhibits the formation of interlocking networks as well as abundant and small Pd nanoparticles formed exclusively on TMV biotemplates. Importantly, the histogram of the Pd nanoparticle sizes based on 100 particles shown in the inset of Figure 3b reflects narrow size distribution of 1.2 ± 0.3 nm in diameter with about 82% of the Pd particles in the size range of 0.6–1.5 nm. Finally, sample with even higher Pd precursor ratio (S7: 10 mM Na_2PdCl_4 and 0.3 mg/mL TMV) in Figure 3c shows large flower-like Pd aggregates outside the TMV biotemplates, while many Pd particles also form on TMV biotemplates with uniform particle size (Figure 2S, Supporting Information). Harris and co-worker[25] also observed large multicrystalline Pd aggregates outside TMV2cys and small Pd clusters along TMV before further sample treatment (washing the sample with deionized water). However, in their study, reducing agent DMAB was used and Pd nanoparticles formed along TMV2cys were not uniform or well-dispersed.

Overall, these results indicate that: (1) certain threshold concentration of Pd precursor is needed for the spontaneous formation of nanoparticles along TMV biotemplates, (2) good dispersion of uniform Pd nanoparticles requires adequate amount of TMV biotemplates, and (3) extra amount of Pd precursor does not lead to the increase in Pd nanoparticle size on TMV biotemplates.

The behavior of Pd nanoparticle formation on TMV biotemplates under various Na_2PdCl_4 and TMV concentrations is summarized in Figure 3d. First, when the Na_2PdCl_4 concentration is as low as 2 mM, no visible Pd nanoparticles were formed on the TMV biotemplates (samples S1 and S2, marked as cross symbols). Second, under certain conditions with adequate concentration and proper ratio of Na_2PdCl_4 and TMV, small Pd nanoparticles form only on TMV biotemplates in a uniform and well-dispersed manner (samples S3, S4, S5, S6 and S9, marked as red round circles). The TEM images of additional samples (S3, S4, S5 and S9) are shown in Figure 1S (Supporting Information), and the average sizes of Pd nanoparticles for those samples are all measured to be between 1 and 2 nm with narrow size distribution (Figure 2S, Supporting Information). Sample S3 and S5 synthesized with the same ratio of Na_2PdCl_4/ TMV (8.3 mmol Pd/g TMV) exhibit nearly the same particle size distribution and average size of 1.7 nm, as shown in Figure 2S, Supporting Information. In addition, in comparison with sample S6 (Na_2PdCl_4/ TMV = 16.6 mmol Pd/g TMV), the decrease in the Na_2PdCl_4/TMV ratio (sample S3 and S5) results in about 1.5-fold decrease in the number of Pd nanoparticles per unit surface area of TMV.

Third, when the TMV concentration is relatively low, large aggregates of Pd particles are found outside TMV biotemplates (samples S7, S8, S10, and S11, marked as triangles in Figure 3d). The TEM images of samples S8, S10, and S11 are also shown in Figure 1S (Supporting Information). Combined, the results summarized in Figure 3d indicate that the concentrations of both Na_2PdCl_4 and TMV, and the ratio between Na_2PdCl_4 and TMV play important roles for the formation of small and uniform Pd nanoparticles along TMV biotemplates, with the optimal ratio of Na_2PdCl_4/TMV(mmol Pd/g TMV) between 6.2 and 17 under the synthesis conditions examined here.

In addition, the effects of incubation time and temperature were also studied as shown in the TEM images of Figures 3S and 4S (Supporting Information). We found that longer incubation time does not lead to changes in Pd particle size or distribution, yet causes certain degree of TMV degradation. Higher incubation temperature (80 °C) shows apparent particle aggregation and does not lead to the increase in Pd particle size. Thus, variation of preparation parameters has minor influence on the Pd size distribution in the presence of TMV, similar to the studies on the formation of colloidal Pd particles in the presence of PVP by Wolf and co-workers.[55]

Finally, the high resolution TEM image of a randomly selected area (Figure 3e) shows that most Pd nanoparticles formed on TMV biotemplates are highly crystalline. The Pd particle in the inset shows 0.22 nm spacing, which corresponds to the (111) interplanar distance of the face centered cubic (fcc) structure of metallic Pd crystals.[56]

The results in Figure 3 exhibit several benefits of TMV as biotemplates for the metal nanoparticle formation. First, TMV provides abundant bioadsorption, nucleation and particle growth sites[22,26,50,57] for the formation of small (1−2 nm) Pd nanoparticles with narrow size distribution under mild aqueous conditions without reducing agents. Specifically, in addition to well-known affinity of cysteine to palladium that enhances the "biosorption" thus nanoparticle formation,[26] other amino acid side chain functionalities (such as tryptophan, aspartic acid, glutamic acid, serine and tyrosine,) are also known to form complexes with metal precursors, and contribute to the controlled formation of metal nanoparticles (*e.g.*, Pd,[58] Ag,[59] and Au[60]).

Second, TMV's robust 3D nanotubular structure keeps the Pd nanoparticles well-dispersed[20,25] throughout centrifugation and resuspension, while the TMV rods form stable networks without aggregation upon Pd metal formation under proper incubation conditions. This network formation of Pd−TMV complexes further facilitates simple separation *via* centrifugation.

Lim *et al.*[31] demonstrated the formation of polycrystalline palladium layers with thickness of 25−35 nm on the outer surface of TMV in the absence of reducer *via* several repeated coating cycles. In our study shown here, ~20-fold higher concentrations of both Na_2PdCl_4 and TMV (within certain synthesis conditions) and only one incubation cycle leads to a completely different behavior, where uniform 1−2 nm Pd nanoparticles are formed in a consistent manner. This spontaneous formation of Pd nanoparticles on TMV may follow complex formation and self-mineralization mechanism, where $PdClx(H_2O)y$ precursors are complexed on the TMV surface functionalities (thiol and hydroxyl groups) and self-mineralized by oxidizing Cl^- to release HClO.[32] Our study here along with previous reports[22,31,32] indicates that the absence of reducing agent in the process leads to slow nanoparticle growth with more uniform crystalline structures. From our observation of the UV−vis absorbance spectra, the formation of Pd−TMV complexes takes as long as 20 min for ~95% of completion. In another report by Lim *et al.*,[32] the incubation time used for the Pd adsorption and mineralization without reducer was also 20 min. In contrast, applying reducer in the TMV solution leads to more rapid and uncontrolled Pd particle formation with some large multicrystalline palladium aggregates outside TMV.[20,22,25,26,50,57] In the Small-Angle X-ray Scattering

(SAXS) study reported by Manocchi *et al.*, [22] the Pd growth on TMV with sodium hypophosphite as the reducer was complete within only 33 s, leading to relatively large (up to 5 nm) Pd particles. Therefore, the reducer-free procedure shown here represents a simple and low-cost approach for the controlled formation of uniform and small Pd nanoparticles along TMV biotemplates.

In summary, results in Figure 3 demonstrate that: (1) small (1−2 nm) and uniform Pd nanoparticles are spontaneously formed along TMV biotemplates without reducing agents, (2) most Pd nanoparticles observed are highly crystalline with (111) facets, and (3) both the concentration and ratio between Na_2PdCl_4 and TMV are important factors for the formation of uniform and well-dispersed Pd−TMV complexes.

Fabrication of Hybrid Hydrogel Microparticles with Encapsulated Pd−TMV Complexes *via* Replica Molding. We next demonstrate that the as-prepared Pd−TMV complexes can be readily integrated into nonspherical, shape-controlled polymeric microparticle formats *via* a simple replica molding (RM) technique, as shown in Figure 4. As shown in the schematic diagram of Figure 4a, the preparticle solution composed of the Pd−TMV complexes, poly(ethylene glycol) diacrylate (PEGDA), PEG200, and photoinitiator (PI) is poured into the PDMS-based micromolds. PEG200 was used as a porogen[61,62] to create porous structure of PEG microparticles to enable the diffusion of reactants and products. The volume ratio of Pd−TMV solution PEGDA/PEG200/PI is set as 55/25/15/5, while the final TMV concentration in the microparticles is varied, as shown in Figure 4d. Upon irradiation with UV light, the preparticle solution undergoes photoinduced radical polymerization to form cross-linked polymeric networks.[63,64]

First, the photographs in Figure 4b show that the preparticle solutions are clear and uniform with final TMV concentration up to 4.8 mg/mL, with increasingly brown color for higher Pd−TMV contents. Next, the photographs of the Pd−TMV embedded PEG microparticles in Figure 4c show increasingly dark color with increasing Pd−TMV contents, indicating that the Pd−TMV complexes are successfully embedded in the PEG hydrogels. Finally, the photomicrographs of the Pd−TMV−PEG microparticles in Figure 4d show uniform color and shape for all the Pd−TMV contents examined up to 4.8 mg/mL TMV concentration without any apparent aggregation or deformation, with highly consistent dimensions of 300 μm in width and 100 μm in thickness from the micromolds. The SEM images in Figure 5S (Supporting Information) also confirm the uniformity of the fabricated microparticles and the smoothness of microparticle surfaces. Various preparticle compositions were also examined for the microparticle fabrication; the microphotographs in Figures 6S and 7S (Supporting Information) clearly show that

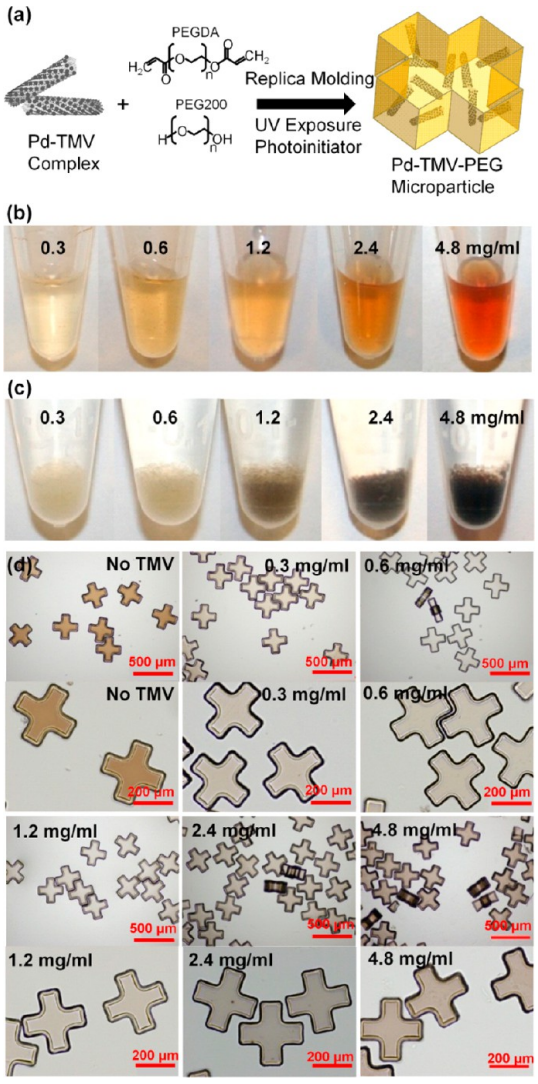

Figure 4. Fabrication of Pd−TMV−PEG microparticles *via* replica molding. (a) Brief schematic diagram of Pd−TMV−PEG microparticle fabrication; (b) photographs of preparticle solutions; (c) photographs of collected Pd−TMV−PEG microparticles from one batch of fabrication; (d) microphotographs of Pd−TMV−PEG microparticles containing various amounts of Pd−TMV complexes. Note: The fabrication condition of all microparticles is PEGDA:PEG200:PI:Pd−TMV (volume ratio) = 25:15:5:55. All the concentrations shown in the images are referred to the TMV concentrations in the preparticle solution.

insufficient concentrations of PEGDA (<15%) and PI (2%) result in incomplete photopolymerization, nonuniform microparticles or low mechanical strength.

Compared to microfluidic techniques for the microparticle fabrication,[50] the results in Figure 4 show many inherent advantages of the RM technique, including simple, robust, and inexpensive procedures as well as scalability and reliable duplication of complex structures.[63] First, the RM procedure is simple and scalable due to the usage of a hand-held UV lamp for photopolymerization rather than a high-intensity UV source requiring delicate control for the photo- or flow-lithographic fabrication procedures.[49,65] Second, the

RM procedure is robust due to the tunable fabrication parameters not limited by needs to maintain consistent flows, viscosity and phase separation. Due to this robustness of the RM procedure, fabrication of multifunctional particles in spatially resolved, multicompartmental formats can also be accomplished without relying on delicate balance of multiple dynamic flows.[66] To illustrate this capability, we have also examined fabrication of Janus particles consisting of two layers as shown in Figure 8S (Supporting Information). The results show that such Janus particles containing catalytically active Pd−TMV complexes and magnetic nanoparticles in two separate phases are readily fabricated in a consistent manner, further illustrating the synergistic advantage of integrating Pd−TMV complexes with RM-based microparticle formats that allows for simple incorporation of additional functionalities. Third, all the silicon master molds, PDMS micromolds, and excess preparticle solution can be fully recycled multiple times, making the RM technique a cost-efficient procedure. Fourth, RM leads to the fabrication of 100% uniform and clean microparticles due to the absence of any continuous phase (*e.g.*, oil and unreacted monomer outside of the objective light)[35] or deformed particles that often arise at the onset and end of each microfluidic procedure. In conclusion, these results clearly demonstrate that the Pd−TMV complexes can be readily integrated into polymeric microparticle formats in a simple and reproducible manner *via* the RM technique.

Catalytic Activity Examination. Next, we examined the catalytic activity of the Pd−TMV−PEG microparticles for Pd nanoparticle-catalyzed dichromate reduction reaction, as shown in Figure 5. For this, Pd−TMV−PEG microparticles (1040 microparticles with total volume of 5.2 μL for each reaction batch) encapsulating various amounts of Pd−TMV complexes (Figure 4) were added to, and vigorously stirred in the 1 mL reaction mixtures containing 0.1 mM $K_2Cr_2O_7$ and 100 mM NaCOOH at pH 3. The conversion was monitored *via* UV−vis spectrophotometry at the dichromate ion's characteristic absorption maximum at 350 nm.

First, as shown in Figure 5a, the bottom conversion curve with star symbol is from the microparticles containing only TMV without Pd nanoparticles, which shows no dichromate conversion. Meanwhile, all the other PEG microparticles containing Pd−TMV complexes show good catalytic activities with the conversions reaching near-completion within the 20 min period. The Pd−TMV−PEG microparticles containing higher Pd loading density clearly show higher conversion rates.

Under the reaction conditions applied, the reaction follows apparent pseudo-first order batch reaction kinetics,[27] and the apparent rate constants k_{app} (min^{-1}) of all batches were obtained from the slope of linear regression of Ln([Cr(VI)]/[Cr(VI)$_0$]) *vs* reaction time,

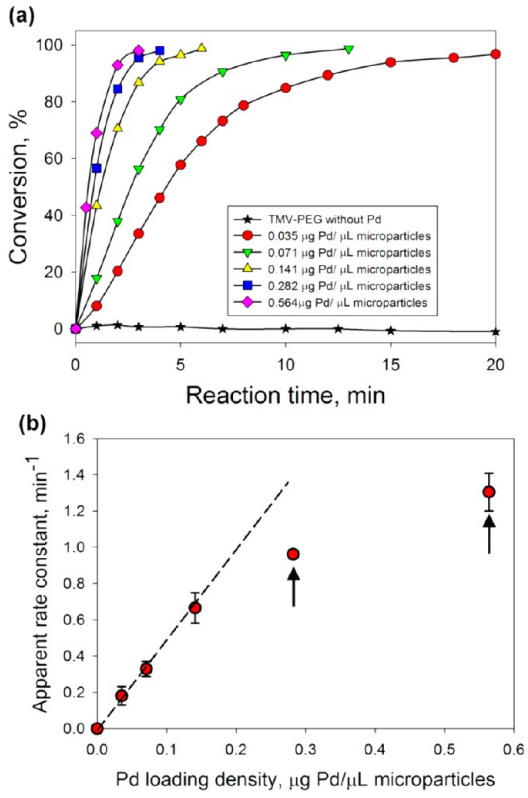

Figure 5. The catalytic activities of Pd−TMV−PEG microparticles encapsulating various amounts of Pd−TMV complexes. (a) Conversion curves of dichromate reduction catalyzed by Pd−TMV−PEG microparticles with different Pd loading densities; (b) Pd loading densities in Pd−TMV−PEG microparticles *versus* apparent reaction rate constants. Note: the Pd loading amount is measured by ICP. Note: preparticle solution composition with ratio of PEGDA: PEG200:PI:Pd−TMV (v/v/v/v) = 25:15:5:55.

where Cr(VI) and Cr(VI)$_0$ represent the dichromate concentration at time t and 0, respectively. Figure 5b shows the average k_{app} from triplicate experiments for the Pd loading density of the microparticles. The small error bars for each condition indicate the high consistency and reproducibility of our synthesis-fabrication procedure. Furthermore, the k_{app} is proportional to the Pd loading density up to Pd loading density of 0.14 μg Pd/μL microparticles (=0.7 ng Pd/each microparticle, as the volume of each microparticle is 5 nanoliter). In this linear region, the observed reaction rate is equal to the intrinsic reaction rate catalyzed by Pd−TMV−PEG microparticles fabricated with composition of PEGDA: PEG200:PI:Pd−TMV (v/v/v/v) = 25:15:5:55, which is calculated to be 98.7 mmol/(g Pd·min) from the first four data points in Figure 5b. Importantly, this observed catalytic activity (normalized by Pd amount) is ~6-fold higher than the commercial Pd/C catalyst, which was determined to be 16.4 ± 0.2 (mmol/(g Pd·min)) (Methods). TEM characterization of commercial 5% Pd/C in Figure 9S (Supporting Information) shows that the carbon-supported Pd particles possess much broader size distribution: average size 3.2 nm with minimum size 1 nm and maximum size 12 nm, with

certain degree of Pd particle aggregation on the carbon support. Thus, the better catalytic performance of Pd−TMV−PEG microparticles than commercial Pd/C catalyst is likely due to the relatively small, uniform, well-dispersed and highly crystalline nature of the Pd nanoparticles on TMV biotemplates.

Next, the apparent rate constants in the linear region (<0.14 μg Pd/μL microparticles) indicate that: (1) all the Pd nanoparticles embedded in the PEG hydrogel network structure are accessible to the reactants for the reaction, 2 the Pd−TMV−PEG microparticles containing uniform and well-dispersed 1−2 nm Pd nanoparticles have good catalytic activity, (3) there appears to be no apparent internal diffusion limitation within these particles containing different Pd−TMV complex amounts, and (4) the PEG network structure provides a good matrix for the encapsulation of catalytically active Pd nanoparticles while allowing for sufficient mass transfer of the small molecule reactants and products under the fabrication conditions enlisted.

When the Pd loading density in the microparticles is above 0.28 μg Pd/μL microparticles (pointed by black arrows), the apparent rate constants k_{app} start becoming lower than the expected ideal ones (dashed line in Figure 5b). This indicates that not all the Pd nanoparticles in the hydrogel microparticles are utilized in the catalytic reaction. One explanation for this deviation from the ideal behavior is that certain degree of internal diffusion limitation occurs in the higher Pd−TMV loading density cases. According to the molecular dynamics (MD) simulations by Wu *et al.*[67] and the Amsden theory,[68] the diffusion coefficient D_{eff} of ions through PEG700 (n = 16) hydrogels is about 0.5×10^{-5} cm^2/s. Thus, the estimation of Weisz modulus (Mw) of the Pd−TMV−PEG microparticles with Pd loading density of 0.28 and 0.56 μg Pd/μL microparticles is about 0.26 and 0.35, respectively. These values of the Weisz modulus are within the range of slight diffusion limitation.[69] The presence of Pd−TMV complexes in cross-linked PEG hydrogel network structure may also change the properties of the hydrogels (such as average mesh size or overall hydrogel structure), thus small degree of internal diffusion limitation may occur for the Pd−TMV−PEG microparticles with higher Pd loading densities.

With robust replica molding technique reported here, these results indicate that the catalyst loading density in hydrogel microparticles can be readily controlled to be in the optimal ranges within the kinetics-controlled regime simply by changing the loading density of the Pd−TMV complexes in the preparticle solution. In addition, the catalytic activity studies in Figure 10S (Supporting Information) show that microparticles fabricated with lower concentration of PEGDA in the preparticle composition exhibit higher apparent rate constant for dichromate reduction. Engberg *et al.*[70,71] found that decreasing the initial PEGDA% acts to increase the spacing of cross-link junctions and to form polymer networks with looser structures. Similarly, the usage of PEG prepolymers with higher molecular weight could lead to larger hydrogel mesh size, resulting in higher diffusion coefficient and thus less internal diffusion limitation of reactants through the polymer matrix.[67]

Meanwhile, the Pd−TMV complexes without encapsulation into the microparticle formats showed substantially lower catalytic activity and aggregation as shown in Figure 11S (Supporting Information). This result further confirms the utility of the integration of Pd−TMV complexes into the PEG hydrogel scaffolds for catalytic reactions, offering significant synergy between the TMV biotemplates that offer small Pd nanoparticle synthesis and dispersion, and the porous hydrogel matrices that offer stable incorporation of otherwise unstable nanobio complexes susceptible to aggregation while allowing ready access to small molecule reactants.

Combined, results in Figure 5 and Figure 11S demonstrate high catalytic activity of the PEG microparticles encapsulating Pd−TMV nanostructures and the significant synergy between Pd−TMV nanobio complex and the porous polymeric matrices. Furthermore, the reaction rate catalyzed by Pd−TMV−PEG microparticles is linearly proportional to the Pd loading density inside hydrogels within the diffusion limitation-free region. Next, the porous network structure of the PEG hydrogels with 2−3 nm mesh size[46] enables sufficient diffusion of small reactant molecules through the matrix. Finally, Pd−TMV−PEG hydrogel microparticles as catalysts allow for simple separation from the reaction solution by low-speed centrifugation or filtration under mild conditions. Therefore, the simple RM technique for fabrication of PEG hydrogel microparticles to encapsulate Pd−TMV complex as catalysts presents a robust strategy that could be readily extended to other hybrid nanostructures or functionalities.

Recyclability and Stability of Pd−TMV−PEG Microparticles. To further examine the stability of the Pd−TMV−PEG microparticles, we next carried out five reaction cycles catalyzed by a single batch of microparticles (total volume = 10.4 μL) containing 0.07 μg Pd/μL microparticles without any regeneration treatments as shown in Figure 6.

The conversion of the dichromate reached near-completion for all the five runs (Figure 6a) with the apparent rate constants being 0.75, 0.77, 0.72, 0.69, and 0.60 min^{-1}, respectively. Considering loss of certain number of microparticles at each recycling (*i.e.*, removal of reaction mixtures), the 20% decrease in the rate constant after 5 reaction cycles indicates stability and recyclability of these hydrogel microparticles under catalytic reaction conditions (*i.e.*, pH 3 and vigorous

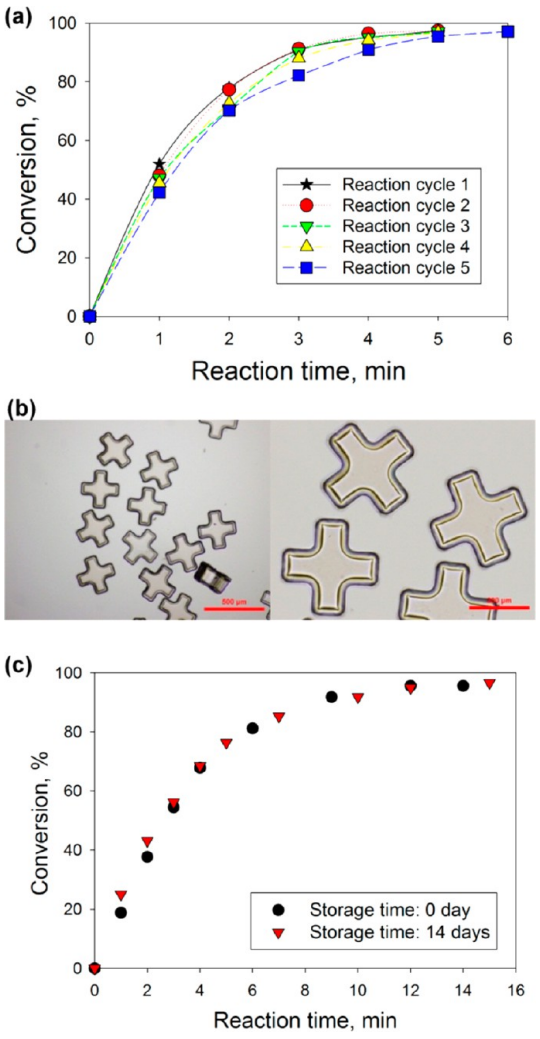

Figure 6. Stability study of Pd−TMV−PEG microparticles as catalysts for dichromate reduction. (a) Recycling study; (b) microphotographs of microparticles after 5 cycles of dichromate reduction; (c) conversion curve of dichromate reduction with microparticles upon 14 days storage.

stirring) employed here. Furthermore, the photomicrographs of the microparticles upon 5 cycle reactions in Figure 6b clearly show that the shape, structure and size remain identical to the before-reaction state. Overall, the results in Figure 6a,b show that the Pd−TMV nanostructures remain entrapped in the cross-linked PEG hydrogel network structure through catalytic reaction conditions in a stable manner. Notably, the good catalytic activity, stability and recyclability of as-prepared Pd−TMV−PEG microparticles as catalysts indicate retention of the Pd−TMV complexes within the polymeric networks mainly due to the relative dimensions of Pd nanoparticles (1−2 nm) *vs* Pd−TMV complexes/network (up to micrometers) *vs* hydrogel mesh size (2−3 nm) *vs* small molecule reactants and products (angstroms). On one hand, the integration of 1−2 nm Pd nanoparticles with TMV nanostructures (in length of 300 nm) allows Pd nanoparticles to stay well-dispersed and entrapped inside the hydrogel networks under catalytic reaction conditions. On the other hand, the 2−3 nm mesh size of hydrogel allows minimal mass transfer limitation of small molecule reactants and products (hydrodynamic radius of a few angstroms) through microparticles with 50 μm characteristic length examined in this study. Hence, TMV biotemplates help the synthesis, dispersion and retention of small Pd nanoparticles within the PEG hydrogel network structure. Furthermore, the microparticle size and mesh size can be readily controlled and manipulated for optimal payload of Pd nanoparticles and catalytic performance.

Finally, we further examined the catalytic activity of the Pd−TMV−PEG microparticles upon long-term storage, as shown in Figure 6c. The conversion rate upon 14-day storage (triangle symbols) at room temperature was identical to the one from freshly prepared samples (circle symbols). This result clearly indicates that the Pd−TMV−PEG microparticles are stable under ambient conditions, and that the PEG hydrogel network provides stable matrix for the Pd−TMV nano-bio complexes without any leaching over extended storage. Combined, results shown in Figure 6 demonstrate that our novel hybrid catalysts embedded in the polymeric microparticle format possess stability under catalytic reaction conditions and upon long-term storage.

CONCLUSIONS

In this study, we have demonstrated and thoroughly examined a facile synthesis−fabrication scheme to create novel nano−bio complexes with small and catalytically active Pd nanoparticles seamlessly integrated in robust polymeric microparticle formats. First, UV−vis absorbance observations showed rapid formation of Pd−TMV complexes that can be readily separated and processed. TEM characterization confirmed the spontaneous and exclusive formation of small (1−2 nm), uniform and highly crystalline Pd(111) nanoparticles along TMV biotemplates. Both concentration and ratio between Na_2PdCl_4 and TMV were found to be important factors for the formation of uniform and well-dispersed Pd nanoparticles. Second, simple and highly reproducible RM procedure enabled integration of Pd−TMV complexes into uniform PEG-based polymeric microparticles. Third, the as-prepared nano-biopolymeric hybrid materials possess readily controllable Pd loading density, high catalytic activity and stability for dichromate reduction reaction. Taken together, these results not only indicate facile routes to harness the unique advantages of biotemplates for the controlled synthesis of functional nanomaterials, but also suggest robust fabrication strategies to integrate additional functionalities in stable, robust and highly reproducible formats. We envision that this novel synthesis−fabrication procedure can be readily

extended to the fabrication of other nanobiopolymeric hybrid materials with multiple functionalities based on various metal nanoparticles or polymer formats for catalysis or energy applications.

METHODS

Materials. The first generation of genetically modified Tobacco Mosaic Virus (TMV1cys) was from Dr. James Culver, at the Institute for Bioscience and Biotechnology Research of University of Maryland Biotechnology Institute. The TMV1cys templates utilized in this study were produced by infecting tobacco plants and extracting from infected tobacco leaves with phosphate extraction buffer, followed by chloroform phase separation, PEG8000 sedimentation and sucrose gradient for TMV purification as previously described.[57] Sodium tetrachloropalladate (II) (Na_2PdCl_4, Sigma-Aldrich, St. Louis, MO) was used as the precursor for the Pd nanoparticle formation. Poly(ethylene glycol) diacrylate (PEG-DA, M_n = 700), PEG (M_n = 200), and 2-hydroxy-2-methylpropiophenone (Darocur 1173, photoinitiator (PI)) were purchased from Sigma-Aldrich (St. Louis, MO). A 0.5% Tween 20 solution was used for microparticle storage. Potassium dichromate ($K_2Cr_2O_7$) (99.5%, Sigma-Aldrich) and sodium formate (HCOONa) (99%, Fisher Scientific, Waltham, MA) were used in the study of dichromate reduction. All of these materials were used as received without further purification.

Spontaneous Formation of Pd Nanoparticles on TMV Biotemplates and Preparticle Solution Preparation. To form Pd nanoparticles on TMV biotemplates, the TMV stock solution was added into the Na_2PdCl_4 solution, then incubated at 50 °C for 30 min. Various concentrations of Na_2PdCl_4 and TMV were studied for the spontaneous formation of Pd nanoparticles on TMV, as shown in Table 1 and Figure 3d. For the catalytic activity study, the Pd–TMV complexes were all synthesized with the condition of sample S6 (0.6 mg/mL TMV, 10 mM Na_2PdCl_4). The mixed solution was centrifuged at 9000*g* for 5 min with a Microfuge 22R centrifuge (Beckman Coulter, Brea, CA). The supernatant was discarded and the collected brown Pd–TMV complex pellets were resuspended in 55 μL of deionized water. After 5 min sonication, the Pd–TMV solution was mixed with 15 μL of PEG200 to make solution **1**. To make solution **2**, 25 μL of PEGDA was thoroughly mixed with 5 μL of PI. Both solutions **1** and **2** were treated with 5 min sonication. Next, solution **1** was added into solution **2** to have 100 μL of preparticle solution with final volume ratio of Pd–TMV solution/PEGDA/PEG200/PI as 55/25/15/5. To make preparticle solutions with TMV final concentration of 0.3, 0.6, 1.2, 2.4, and 4.8 mg/mL, varying volumes of the Pd–TMV solutions (0.6 mg/mL TMV, 10 mM Na_2PdCl_4) at 50, 100, 200, 400, and 800 μL were centrifuged, and the collected pellets were resuspended in 55 μL of DI water, mixed with PEG200, then added to solution **2** to obtain 100 μL of total volume of preparticle solutions.

Fabrication of Pd–TMV–PEG Microparticles *via* Replica Molding. The four major steps of soft lithography, as described by others,[72] were followed to prepare the microparticles. Briefly, AutoCAD was used to design the shaped patterns. High-resolution printing was used to generate photomasks on transparency films for the fabrication of silicon masters *via* photolithography. PDMS elastomeric micromolds were formed with Sylgard 184 (Dow Corning, Midland, MI) following a 24 h cure at 65 °C. Finally, microparticles were fabricated from the PDMS elastomeric micromolds *via* replica molding (RM).

As shown in Figure 1, prepolymer solution (100 μL) was first placed on the surface of the PDMS micromolds (2080 wells per 2 cm × 2 cm mold). Each cross-shape microparticle has arms of length 100 μm, depth of 100 μm and total width of 300 μm. The volume of each well is 5 nL. The air bubbles in the microwells were removed by rubbing plastic pipet tips against the PDMS molds. After the removal of the excess preparticle solution, the filled PDMS micromolds were then sealed in a humidity chamber (≥90% relative humidity) with a glass slide coated with a thin layer of PDMS obtained *via* spin-coating for 30 s at 1000 rpm. A square section (same size as the microwell square region within the micromold) of PDMS of this slide had been removed from the glass slide to provide a small gap between the glass surface and the top portion of the microwells. The sealed micromolds were then placed on an aluminum mirror (Thorlabs, Newton, NJ) and exposed to 365 nm UV light with an 8 W hand-held UV lamp (Spectronics Corp., Westbury, NY) for 15 min. The polymerized PEG microparticles with encapsulated Pd–TMV complexes (Pd–TMV–PEG microparticles) were collected from the microwells by first physically bending the mold, then placing water containing 0.5% (v/v) Tween 20 on the mold surface. The microparticles were collected by pipetting up and down a few times before transferring into a storage vial. This particle removal with water was repeated several times for the complete collection of microparticles. The prepared Pd–TMV–PEG microparticles are stored in 0.5% (v/v) Tween 20 solution at room temperature until catalytic reaction studies.

High-Resolution Transmission Electron Microscopy (HRTEM) Characterization. The samples for the HRTEM characterizations were prepared as follows: 10 μL of well-dispersed Pd–TMV solution was placed onto 300 mesh copper grid carbon TEM grids (FCF300-Cu, EMS Sciences, Hatfield, PA), and left to dry before examination. The TEM analysis was carried out on a JEOL 2100 TEM at 200 keV at the Center for Nanoscale Systems (CNS) at Harvard University (Cambridge, MA).

Imaging Analysis. The Pd–TMV–PEG microparticles were visualized with an Olympus BX51 microscope (Chroma Technology Corp., Rockingham, VT), and the brightfield micrographs were captured with a DP70 microscope digital camera.

Inductively Coupled Plasma Atomic Emission Spectroscopy (ICP-OES). The Pd loading densities of the Pd–TMV–PEG hydrogel microparticles containing various TMV concentrations were determined by ICP-OES. For this, before hydrogel encapsulation, centrifuged Pd–TMV complex pellets were mixed with aqua regia solution (HCl:HNO_3 (v/v) = 4:1) for acid digestion. After complete dissolution of Pd–TMV complexes for about 5 min, the acid-digested solutions were analyzed by Perkin-Elmer 7300 ICP-OES (PerkinElmer, Inc., Waltham, MA). As shown in Table 2, the Pd loading densities of the Pd–TMV–PEG microparticles with various concentrations of TMV were determined based on the Pd amounts added into the preparticle solutions.

TABLE 1. Synthesis Conditions of Pd Spontaneous Formation on TMV Biotemplates

sample number	Na_2PdCl_4, mM	TMV1cys, mg/mL	ratio between Pd/TMV
S1	2.0	1.6	1.3
S2	2.0	0.12	16
S3	5.0	0.60	8.3
S4	10	1.6	6.4
S5	10	1.2	8.3
S6	10	0.60	17
S7	10	0.30	33
S8	15	0.60	25
S9	20	1.6	13
S10	20	0.12	160

TABLE 2. The Pd Loading Densities of Pd–TMV–PEG Microparticles with Various TMV Concentrations

TMV concentration inside microparticles, mg/mL	0	0.30	0.60	1.2	2.4	4.8
Pd loading density, μg Pd/μL microparticles	0	0.035	0.071	0.14	0.28	0.56

Catalytic Activity Examination of Pd–TMV–PEG Microparticles. Dichromate reduction was employed to examine the catalytic activity of Pd–TMV–PEG microparticles. For this, microparticles (total volume = 5.2 μL) was added into 1 mL reaction solution containing 0.1 mM potassium dichromate and 100 mM sodium formate at pH 3. The coupled redox reactions are enumerated in eqs 1 and 2. The reaction was monitored *in situ* with Evolution 300 UV/vis Spectrophotometer (Thermo scientific, Waltham, MA) every minute at 350 nm, the characteristic absorption maximum of the dichromate ion.

$$Cr_2O_7^{2-} + 14H_3O^+ + 6e^- \leftrightarrow 2Cr^{3+} + 21H_2O \quad (1)$$

$$HCOOH + 2H_2O \leftrightarrow CO_2 + 2H_3O^+ + 2e^- \quad (2)$$

The absorbance at 350 nm was used to calculate Cr(VI) ion concentration, using a calibration curve derived from standard solutions. The conversion of Cr(VI) was calculated from $([Cr(VI)_0] - [Cr(VI)])/Cr(VI)_0 \times 100\%$, where $[Cr(VI)_0]$ is the original concentration before reaction and [Cr(VI)] is the concentration at each time point. The reaction can be considered to follow pseudo-first-order kinetics under the reaction conditions in this study. From the linear regression of $Ln([Cr(VI)]/[Cr(VI)_0])$ *vs* reaction time, the obtained slope represents the apparent first-order rate constant.[27] The initial reaction rates r (mmol/min) were obtained from the slope of the dichromate concentration *vs* time plots during the initial reaction period, *i.e.*, initial rate

$$r = -\frac{dC}{dt} = -\frac{\Delta C}{\Delta t} = -\frac{C_{(t=1\text{min})} - C_{(t=0\text{min})}}{(t_{1\text{min}} - t_{0\text{min}})}$$

For the examination of pore diffusion effects, Weisz modulus Mw was calculated by the eq 3 shown below.

$$Mw = -\frac{r_A \times L^2}{C_A \times D_{eff}} \quad (3)$$

where r_A is the observed reaction rate (mol/(m^3 solid · s)), L is the characteristic length of microparticles (50 μm in our study), C_A is the concentration of dichromate in the solution, D_{eff} is the diffusion coefficient of reactants.

Catalytic Activity Comparison with Commercial Pd/C Catalysts. For direct catalytic activity comparison with Pd–TMV–PEG microparticles, 2.3 mg of commercial 5% Pd/C catalysts was immersed in 40 mL of the standard dichromate solution (with the same condition used for Pd–TMV–PEG microparticles as described in the previous section). The reaction rate was then closely monitored *via* UV–vis. At each time point (every 1 min), a small volume (0.5 mL) of the reaction solution was removed and filtered with a syringe filter (pore size = 0.22 μm, diameter = 13 mm, Polypropylene Housing, VWR); the absorbance of the supernatant at 350 nm was measured. For comparison purposes, the dichromate reduction initial rates catalyzed by both catalyst systems, 5% Pd/C and Pd–TMV–PEG microparticles, were each normalized by the Pd metal contents (mass). The unit of the normalized initial reaction rate per unit Pd mass is mmol/(g Pd · min).

Conflict of Interest: The authors declare no competing financial interest.

Acknowledgment. We gratefully acknowledge financial support from the U.S. National Science Foundation under Grant No. CBET-0941538, Stanley Charm fellowship (C.Y.) and the National Research Foundation of Korea (NRF) grant funded by the Korean government (MEST, No. 2011-0017322). The TEM measurements were performed at the Center for Nanoscale Systems (CNS) in Harvard University, a member of the National Nanotechnology Infrastructure Network (NNIN), which is supported by the National Science Foundation under NSF award no. ECS-0335765. The authors also thank Dr. Y. Lin (Tufts University, Biomedical Engineering Department) for assistance with SEM.

Supporting Information Available: Additional TEM images of Pd–TMV complex, size distribution of Pd nanoparticles, effect of incubation time and temperature on Pd formation, Scanning Electron Microscope characterization, effect of preparticle solution composition on microparticle formation and catalytic activities, characterization of commercial 5% Pd/C catalysts *via* TEM, Janus microparticle fabrication, and negative control catalytic reaction studies with Pd–TMV complexes without encapsulation into PEG microparticle formats. This material is available free of charge *via* the Internet at http://pubs.acs.org.

REFERENCES AND NOTES

1. Hutchings, G. J. Nanocrystalline Gold and Gold Palladium Alloy Catalysts for Chemical Synthesis. *Chem. Commun.* **2008**, *10*, 1148–1164.
2. Rao, C. R. K.; Trivedi, D. C. Chemical and Electrochemical Depositions of Platinum Group Metals and Their Applications. *Coord. Chem. Rev.* **2005**, *249*, 613–631.
3. Zhang, W. Nanoscale Iron Particles for Environmental Remediation: An Overview. *J. Nanopart. Res.* **2003**, *5*, 323–332.
4. Drelinkiewicza, A.; Waksmundzka, A.; Makowski, W.; Sobczak, J. W.; Król, A.; Zieba, A. Acetophenone Hydrogenation on Polymer–Palladium Catalysts. The Effect of Polymer Matrix. *Catal. Lett.* **2004**, *94*, 143–156.
5. Nobre, S. M.; Monteiro, A. L. Pd Complexes of Iminophosphine ligands: A Homogeneous Molecular Catalyst for Suzuki-Miyaura Cross-coupling Reactions under Mild Conditions. *J. Mol. Catal. A: Chem.* **2009**, *313*, 65–73.
6. Polshettiwar, V.; Len, C.; Fihri, A. Silica-Supported Palladium: Sustainable Catalysts for Cross-coupling Reactions. *Coord. Chem. Rev.* **2009**, *253*, 2599–2626.
7. Martinez, S.; Moreno-Manas, M.; Vallribera, A.; Schubert, U.; Roig, A.; Molins, E. Highly Dispersed Nickel and Palladium Nanoparticle Silica Aerogels: Sol-Gel Processing of Tethered Metal Complexes and Application as Catalysts in the Mizoroki-Heck Reaction. *New J. Chem.* **2006**, *30*, 1093–1097.
8. Das, D. D.; Sayari, A. Applications of Pore-Expanded Mesoporous Silica 6. Novel Synthesis of Monodispersed Supported Palladium Nanoparticles and Their Catalytic Activity for Suzuki Reaction. *J. Catal.* **2007**, *246*, 60–65.
9. Chen, X.; Hou, Y.; Wang, H.; Cao, Y.; He, J. Facile Deposition of Pd Nanoparticles on Carbon Nanotube Microparticles and Their Catalytic Activity for Suzuki Coupling Reactions. *J. Phys. Chem. C* **2008**, *112*, 8172–8176.
10. Young, M.; Willits, D.; Uchida, M.; Douglas, T. Plant Viruses as Biotemplates for Materials and Their Use in Nanotechnology. *Annu. Rev. Phytopathol.* **2008**, *46*, 361–384.
11. Huang, Y.; Chiang, C. Y.; Lee, S. K.; Gao, Y.; Hu, v. L.; Yoreo, J. D.; Belcher, A. M. Programmable Assembly of Nanoarchitectures Using Genetically Engineered Viruses. *Nano Lett.* **2005**, *5*, 1429–1434.
12. Blum, A. S.; Soto, C. M.; Wilson, C. D.; Cole, J. D.; Kim, M.; Gnade, B.; Chatterji, A.; Ochoa, W. F.; Lin, T.; Johnson, J. E.; *et al.* Cowpea Mosaic Virus as a Scaffold for 3-D Patterning of Gold Nanoparticles. *Nano Lett.* **2004**, *4*, 867–870.
13. Douglas, T.; Strable, E.; Willits, D.; Aitouchen, A.; Libera, M.; Young, M. Protein Engineering of a Viral Cage for Constrained Nanomaterials Synthesis. *Adv. Mater.* **2002**, *14*, 415–418.
14. Knez, M.; Bittner, A. M.; Boes, F.; Wege, C.; Jeske, H.; Maiβ, E.; Kern, K. Biotemplate Synthesis of 3-nm Nickel and Cobalt Nanowires. *Nano Lett.* **2003**, *3*, 1079–1082.
15. Aljabali, A. A. A.; Barclay, J. E.; Lomonossoff, G. P.; Evans, D. J. Virus Templated Metallic Nanoparticles. *Nanoscale* **2010**, *2*, 2596–2600.
16. Kramer, R. M.; Li, C.; Carter, D. C.; Stone, M. O.; Naik, R. R. Engineered Protein Cages for Nanomaterial Synthesis. *J. Am. Chem. Soc.* **2004**, *126*, 13282–13286.
17. Douglas, T.; Stark, V. T. Nanophase Cobalt Oxyhydroxide Mineral Synthesized within the Protein Cage of Ferritin. *Inorg. Chem.* **2000**, *39*, 1828–1830.
18. San, B. H.; Kim, S.; Moh, S. H.; Lee, H.; Jung, D.-Y.; Kim, K. K. Platinum Nanoparticles Encapsulated by Aminopeptidase: A Multifunctional Bioinorganic Nanohybrid Catalyst. *Angew. Chem., Int. Ed.* **2011**, *50*, 11924–11929.

19. Dujardin, E.; Peet, C.; Stubbs, G.; Culver, J. N.; Mann, S. Organization of Metallic Nanoparticles Using Tobacco Mosaic Virus Templates. *Nano Lett.* **2003**, *3*, 413–417.
20. Knez, M.; Sumser, M.; Bittner, A. M.; Wege, C.; Jeske, H.; Martin, T. P.; Kern, K. Spatially Selective Nucleation of Metal Clusters on the Tobacco Mosaic Virus. *Adv. Funct. Mater* **2004**, *14*, 116–124.
21. Lee, S. Y.; Choi, J.; Royston, E.; B.Janes, D.; N.Culver, J.; Harris, M. T. Deposition of Platinum Clusters on Surface-Modified Tobacco Mosaic Virus. *J. Nanosci. Nanotechnol.* **2006**, *6*, 974–981.
22. Manocchi, A. K.; Seifert, S.; Lee, B.; Yi, H. *In Situ* Small-Angle X-ray Scattering Analysis of Palladium Nanoparticle Growth on Tobacco Mosaic Virus Nanotemplates. *Langmuir* **2011**, *27*, 7052–7058.
23. Shenton, W.; Douglas, T.; Young, M.; Stubbs, G.; Mann, S. Inorganic-organic Nanotube Composites from Template Mineralization of Tobacco Mosaic Virus. *Adv. Mater.* **1999**, *11*, 253–256.
24. Lim, J.-S.; Kim, S.-M.; Lee, S.-Y.; Stach, E. A.; Culver, J. N.; Harris, M. T. Formation of Au/Pd Alloy Nanoparticles on TMV. *J. Nanomater.* **2010**, *2010*, 1–7.
25. Lee, S.; Royston, E.; Culver, J. N.; Harris, M. T. Improved Metal Cluster Deposition on a Genetically Engineered Tobacco Mosaic Virus Template. *Nanotechnol.* **2005**, *16*, S435–S441.
26. Lim, J.-S.; Kim, S.-M.; Lee, S.-Y.; Stach, E. A.; Culver, J. N.; Harris, M. T. Quantitative Study of Au(III) and Pd(II) Ion Biosorption on Genetically Engineered Tobacco Mosaic Virus. *J. Colloid Interface Sci.* **2010**, *342*, 455–461.
27. Yang, C.; Manocchi, A. K.; Lee, B.; Yi, H. Viral Templated Palladium Nanocatalysts for Dichromate Reduction. *Appl. Catal., B* **2010**, *93*, 282–291.
28. Yang, C.; Manocchi, A. K.; Lee, B.; Yi, H. Viral-Templated Palladium Nanocatalysts for Suzuki Coupling Reaction. *J. Mater. Chem.* **2011**, *21*, 187–194.
29. Yang, C.; Yi, H. Facile Approaches to Control Catalytic Activity of Viral-templated Palladium Nanocatalysts for Dichromate Reduction. *Biochem. Eng. J.* **2010**, *52*, 160–167.
30. Manocchi, A. K.; Horelik, N. E.; Lee, B.; Yi, H. Simple, Readily Controllable Palladium Nanoparticle Formation on Surface-Assembled Viral Nanotemplates. *Langmuir* **2010**, *26*, 3670–3677.
31. Lim, J.-S.; Kim, S.-M.; Lee, S.-Y.; Stach, E. A.; Culver, J. N.; Harris, M. T. Biotemplated Aqueous-Phase Palladium Crystallization in the Absence of External Reducing Agents. *Nano Lett.* **2010**, *10*, 3863–3867.
32. Lim, J.-S.; Kim, S.-M.; Lee, S.-Y.; Stach, E. A.; Culver, J. N.; Harris, M. T. Surface Functionalized Silica as a Toolkit for Studying Aqueous Phase Palladium Adsorption and Mineralization on Thiol Moiety in the Absence of External Reducing Agents. *J. Colloid Interface Sci.* **2011**, *356*, 31–36.
33. Shakeri, M.; Tai, C. W.; Gothelid, E.; Oscarsson, S.; Backvall, J. E. Small Pd Nanoparticles Supported in Large Pores of Mesocellular Foam: An Excellent Catalyst for Racemization of Amines. *Chemistry* **2011**, *17*, 13269–13273.
34. Wang, Y.; Yan, R.; Zhang, J.; Zhang, W. Synthesis of Efficient and Reusable Catalyst of Size-Controlled Au Nanoparticles within a Porous, Chelating and Intelligent Hydrogel for Aerobic Alcohol Oxidation. *J. Mol. Catal. A: Chem.* **2010**, *317*, 81–88.
35. Yuet, K. P.; Hwang, D. K.; Haghgooie, R.; Doyle, P. S. Multifunctional Superparamagnetic Janus Particles. *Langmuir* **2009**, *26*, 4281–4287.
36. Klem, M. T.; Young, M.; Douglas, T. Biomimetic Synthesis of β-TiO2 inside A Viral Capsid. *J. Mater. Chem.* **2008**, *18*, 3821–3823.
37. Butun, S.; Sahiner, N. A Versatile Hydrogel Template for Metal Nano Particle Preparation and Their Use in Catalysis. *Polymer* **2011**, *52*, 4834–4840.
38. Mohan, Y. M.; Premkumar, T.; Lee, K.; Geckeler, K. E. Fabrication of Silver Nanoparticles in Hydrogel Networks. *Macromol. Rapid Commun.* **2006**, *27*, 1346–1354.
39. Sahiner, N.; Ozay, H.; Ozay, O.; Aktas, N. New Catalytic Route: Hydrogels as Templates and Reactors for *in situ* Ni Nanoparticle Synthesis and Usage in the Reduction of 2-and 4-Nitrophenols. *Appl. Catal., A* **2010**, *385*, 201–207.
40. Lu, Y.; Spyra, P.; Mei, Y.; Ballauff, M.; Pich, A. Composite Hydrogels: Robust Carriers for Catalytic Nanoparticles. *Macromol. Chem. Phys.* **2007**, *208*, 254–261.
41. Hou, Z.; Theyssen, N.; Brinkmann, A.; Leitner, W. Biphasic Aerobic Oxidation of Alcohols Catalyzed by Poly(Ethylene Glycol)-Stabilized Palladium Nanoparticles in Supercritical Carbon Dioxide. *Angew. Chem., Int. Ed.* **2005**, *117*, 1370–1373.
42. Hou, Z.; Theyssen, N.; Leitner, W. Palladium Nanoparticles Stabilised on PEG-modified Silica as Catalysts for the Aerobic Alcohol Oxidation in Supercritical Carbon Dioxide. *Green Chem.* **2007**, *9*, 127–132.
43. Harraz, F. A.; El-Hout, S. E.; Killa, H. M.; Ibrahim, I. A. Palladium Nanoparticles Stabilized by Polyethylene Glycol: Efficient, Recyclable Catalyst for Hydrogenation of Styrene and Nitrobenzene. *J. Catal.* **2012**, *286*, 184–192.
44. Huang, T. S.; Wang, Y. H.; Jiang, J. Y.; Jin, Z. L. PEG-Stabilized Palladium Nanoparticles: An Efficient and Recyclable Catalyst for the Selective Hydrogenation of 1,5-Cyclooctadiene in Thermoregulated PEG Biphase System. *Chin. Chem. Lett.* **2008**, *19*, 102–104.
45. Luo, C.; Zhang, Y.; Wang, Y. Palladium Nanoparticles in Poly(ethyleneglycol): The Efficient and Recyclable Catalyst for Heck Reaction. *J. Mol. Catal. A: Chem.* **2005**, *229*, 7–12.
46. Cruise, G. M.; Scharp, D. S.; Hubbell, J. A. Characterization of Permeability and Network Structure of Interfacially Photopolymerized Poly(Ethylene Glycol) Diacrylate Hydrogels. *Biomater.* **1998**, *19*, 1287–1294.
47. Odian, G. *Principles of Polymerization*; John Wiley & Sons: Hoboken, NJ, 2004.
48. Owlad, M.; Aroua, M.; Daud, W.; Baroutian, S. Removal of Hexavalent Chromium-Contaminated Water and Wastewater: A Review. *Water, Air, Soil Pollut.* **2009**, *200*, 59–77.
49. Dhananjay, D.; Patrick, S. D. The Synthesis and Assembly of Polymeric Microparticles Using Microfluidics. *Adv. Mater.* **2009**, *21*, 4071–4086.
50. Lewis, C. L.; Lin, Y.; Yang, C.; Manocchi, A. K.; Yuet, K. P.; Doyle, P. S.; Yi, H. Microfluidic Fabrication of Hydrogel Microparticles Containing Functionalized Viral Nanotemplates. *Langmuir* **2010**, *26*, 13436–13441.
51. Nam, Y. S.; Magyar, A. P.; Lee, D.; Kim, J.-W.; Yun, D. S.; Park, H.; Pollom, T. S.; Weitz, D. A.; Belcher, A. M. Biologically Templated Photocatalytic Nanostructures for Sustained Light-Driven Water Oxidation. *Nat. Nanotechnol.* **2010**, *5*, 340–344.
52. Tong, L.; Righini, M.; Gonzalez, M. U.; Quidant, R.; Kall, M. Optical Aggregation of Metal Nanoparticles in a Microfluidic Channel for Surface-Enhanced Raman Scattering Analysis. *Lab Chip* **2009**, *9*, 193–195.
53. Wang, H.-F.; Kaden, W. E.; Dowler, R.; Sterrer, M.; Freund, H.-J. Model Oxide-Supported Metal Catalysts - Comparison of Ultrahigh Vacuum and Solution Based Preparation of Pd Nanoparticles on a Single-Crystalline Oxide Substrate. *Phys. Chem. Chem. Phys.* **2012**, *14*, 11525–11533.
54. Elding, L. I. Palladium(II) Halide Complexes. I. Stabilities and Spectra of Palladium(II) Chloro and Bromo Aqua Complexes. *Inorg. Chim. Acta* **1972**, *6*, 647–651.
55. Klasovsky, F.; Claus, P.; Wolf, D. Influence of Preparation Parameters on the Performance of Colloid-Derived Oxidic Palladium Catalysts for Selective Hydrogenation of C−C Triple Bonds. *Top. Catal.* **2009**, *52*, 412–423.
56. Xiong, Y.; Chen, J.; Wiley, B.; Xia, Y.; Yin, Y.; Li, Z.-Y. Size-Dependence of Surface Plasmon Resonance and Oxidation for Pd Nanocubes Synthesized *via* a Seed Etching Process. *Nano Lett.* **2005**, *5*, 1237–1242.
57. Yi, H.; Nisar, S.; Lee, S.; Powers, M. A.; Bentley, W. E.; Payne, G. F.; Ghodssi, R.; Rubloff, G. W.; Harris, M. T.; Culver, J. N. Patterned Assembly of Genetically Modified Viral Nanotemplates *via* Nucleic Acid Hybridization. *Nano Lett.* **2005**, *5*, 1931–1936.

58. Chiu, C. Y.; Li, Y.; Huang, Y. Size-Controlled Synthesis of Pd Nanocrystals Using a Specific Multifunctional Peptide. *Nanoscale* **2010**, *2*, 927–930.
59. Nam, K. T.; Lee, Y. J.; Krauland, E. M.; Kottmann, S. T.; Belcher, A. M. Peptide-Mediated Reduction of Silver Ions on Engineered Biological Scaffolds. *ACS Nano* **2008**, *2*, 1480–1486.
60. Toroz, D.; Corni, S. Peptide Synthesis of Gold Nanoparticles: The Early Steps of Gold Reduction Investigated by Density Functional Theory. *Nano Lett.* **2011**, *11*, 1313–1318.
61. Appleyard, D. C.; Chapin, S. C.; Srinivas, R. L.; Doyle, P. S. Bar-Coded Hydrogel Microparticles for Protein Detection: Synthesis, Assay and Scanning. *Nat. Protocols* **2011**, *6*, 1761–1774.
62. Choi, N. W.; Kim, J.; Chapin, S. C.; Duong, T.; Donohue, E.; Pandey, P.; Broom, W.; Hill, W. A.; Doyle, P. S. Multiplexed Detection of mRNA Using Porosity-Tuned Hydrogel Microparticles. *Anal. Chem.* **2012**, *84*, 9370–9378.
63. Lewis, C. L.; Choi, C.-H.; Lin, Y.; Lee, C.-S.; Yi, H. Fabrication of Uniform DNA-Conjugated Hydrogel Microparticles *via* Replica Molding for Facile Nucleic Acid Hybridization Assays. *Anal. Chem.* **2010**, *82*, 5851–5858.
64. Perry, J. L.; Herlihy, K. P.; Napier, M. E.; Desimone, J. M. PRINT: A Novel Platform toward Shape and Size Specific Nanoparticle Theranostics. *Acc. Chem. Res.* **2011**, *44*, 990–998.
65. Xu, S.; Nie, Z.; Seo, M.; Lewis, P.; Kumacheva, E.; Stone, H. A.; Garstecki, P.; Weibel, D. B.; Gitlin, I.; Whitesides, G. M. Generation of Monodisperse Particles by Using Microfluidics: Control over Size, Shape, and Composition. *Angew. Chem., Int. Ed.* **2005**, *44*, 724–728.
66. Choi, C.-H.; Lee, J.; Yoon, K.; Tripathi, A.; Stone, H. A.; Weitz, D. A.; Lee, C.-S. Surface-Tension-Induced Synthesis of Complex Particles Using Confined Polymeric Fluids. *Angew. Chem., Int. Ed.* **2010**, *49*, 7748–7752.
67. Wu, Y.; Joseph, S.; Aluru, N. R. Effect of Cross-Linking on the Diffusion of Water, Ions, and Small Molecules in Hydrogels. *J. Phys. Chem. B* **2009**, *113*, 3512–3520.
68. Amsden, B. Solute Diffusion within Hydrogels. Mechanisms and Models. *Macromolecules* **1998**, *31*, 8382–8395.
69. Levenspiel, O. *The Chemical Reactor Omnibook*; Oregon St Univ Bookstores: Corvallis, OR, 2002.
70. Engberg, K.; Frank, C. W. Protein Diffusion in Photopolymerized Poly(ethylene glycol) Hydrogel Networks. *Biomed. Mater.* **2011**, *6*, 26.
71. Lee, W.; Cho, N.-J.; Xiong, A.; Glenn, J. S.; Frank, C. W. Hydrophobic Nanoparticles Improve Permeability of Cell-Encapsulating Poly(ethylene glycol) Hydrogels while Maintaining Patternability. *Proc. Nat. Acad. Sci. U.S.A.* **2010**, *107*, 20709–20714.
72. Qin, D.; Xia, Y.; Whitesides, G. M. Soft Lithography for Micro- and Nanoscale Patterning. *Nat. Protocols* **2010**, *5*, 491–502.